Research Square

Preprints are preliminary reports that have not undergone peer review.
They should not be considered conclusive, used to inform clinical practice,
or referenced by the media as validated information.

Observation of robust corner states in photonic crystals without global symmetries

Zhi-Yuan Li

phzyli@scut.edu.cn

South China University of Technology https://orcid.org/0000-0003-4692-5028

Zitao Ji

Singapore University of Technology and Design

Jianfeng Chen

National University of Singapore https://orcid.org/0000-0002-9088-2750

Yidong Zheng

South China University of Technology

Zhaogang Dong

Singapore University of Technology and Design https://orcid.org/0000-0002-0929-7723

Article

Keywords:

Posted Date: September 11th, 2026

DOI: https://doi.org/10.21203/rs.3.rs-10862634/v1

License: This work is licensed under a Creative Commons Attribution 4.0 International License.
Read Full License

Additional Declarations: There is **NO** Competing Interest.

Abstract

Robust corner states have attracted considerable attention in recent years, particularly in photonic systems. They are typically realized in second-order topological insulators, including shrunken-expanded lattices and breathing Kagome lattices, where global symmetries are essential in their formation. This reliance on symmetry, however, can make these states highly sensitive to structural disorder. Here, we propose and experimentally demonstrate a class of robust corner states in photonic crystals that require neither global symmetry nor nontrivial topology. By locally tailoring the corner geometry of an otherwise topologically trivial structure, we create strongly localized modes that remain stable under both position and radius disorder. These states are not accidental; rather they originate from a pair of Dirac points in the bulk band structure. Geometric tuning shifts the flatband edge states connecting the Dirac points into an otherwise trivial bandgap, thereby inducing strongly localized corner states. Our findings uncover a previously overlooked class of symmetry-independent, disorder-resilient corner states, extend robust localization beyond conventional topological protection, and provide a route toward light localization in all-dielectric photonic systems.

Introduction

Robust corner states have emerged as a hallmark of second-order topological insulators, which generalize the conventional bulk-boundary correspondence by supporting boundary modes of codimension two[1–10]. In two-dimensional second-order topological insulators, these higher-codimension modes appear as zero-dimensional corner states[11–16]. Originally conceived for electronic systems, such second-order topological phases have since been extended to a broad range of other physical platforms, including photonic systems[3,17–29], acoustic systems[30–32], thermal metamaterials[33–35], electrical circuits[36–38], and ultracold atoms[39]. In photonic systems, two widely studied design paradigms have been employed to realize robust corner states. The first employs shrunken-expanded lattices, in which lattice deformations drive band inversions and alter quantized bulk multipole moments or edge polarizations, as characterized by Zak phases or related crystalline topological indices[3,22–24,29]. The second employs breathing Kagome lattices, in which corner states are associated with an obstructed atomic limit characterized by a mismatch between the Wannier centers and the physical lattice sites[25–28]. These zero-dimensional corner-localized modes offer promising opportunities for applications including topological lasers[40–45] and rainbow trapping[46,47], highlighting their versatility and potential for integrated photonics.

The conventional understanding is that robust corner states in higher-order topological phases generally rely on global crystalline symmetries, which quantize the relevant bulk or edge topological indices and constrain the corner modes. This reliance can make such states particularly sensitive to structural disorder that breaks the protecting symmetries. Rather than being immediately destroyed by any symmetry-breaking perturbation, their eigenfrequencies may shift, and their localization may eventually be lost through hybridization with edge or bulk continua. This vulnerability contrasts with that of first-

order topological boundary states in systems such as Chern and $\mathbb{Z}_2$ insulators, which can survive substantial disorder provided that the bulk or mobility gap remains open and, in the $\mathbb{Z}_2$ case, time-reversal symmetry is preserved. This contrast raises a more fundamental question: must robust corner localization necessarily rely on global crystalline-symmetry protection? Recent theoretical work has shown that non-Hermiticity can provide an intrinsic mechanism for generating localized zero modes without global crystalline-symmetry protection[48]. In such systems, however, localization relies on explicitly non-Hermitian ingredients, such as asymmetric gain/loss or nonreciprocal coupling. Whether analogous symmetry-independent corner localization can be achieved in a fully Hermitian system, without relying on gain/loss, nonreciprocity, or other non-Hermitian effects, remains largely unexplored.

Here, we demonstrate a route to robust corner localization in Hermitian systems that is independent of global crystalline-symmetry protection. Our key finding is that the flatband edge states connecting the boundary projections of a pair of bulk Dirac points can be spectrally shifted through boundary engineering. Conventionally, corner states are obtained by breaking lattice symmetry or modulating intercell couplings, thereby lifting the Dirac-point degeneracy and opening a topological nontrivial bandgap (Figs. 1a-1b). Once the gap opens, the pre-existing flatband edge states persist within the newly opened gap, providing the in-gap boundary states from which corner states emerge. Opening a gap at the Dirac points, however, is not required. Instead, boundary engineering can shift these Dirac-connected flatband edge states into a separate, topologically trivial bandgap, thereby generating robust edge and corner states (Fig. 1c). Tight-binding calculations reveal that tuning an on-site mass term M_s at the boundary of a Dirac semimetal shifts these flatband edge states from their original spectral region between the projected Dirac points, through the upper bulk band, and into the trivial bandgap (Figs. 1d-1e). Joining two such engineered boundaries to form a corner then gives rise to a corner-localized state (Figs. 1f-1g). The resulting corner states evolve from the Dirac-connected edge states rather than from isolated defect modes and require neither higher-order bulk topology nor global crystalline-symmetry protection[1,11,49–52]. A detailed comparison is provided in Table S1 of Supplementary Note 4. Notably, in electronic systems, these flatband edge states may lie far from the Fermi level, limiting their direct contribution to low-energy responses. This constraint does not apply to photonic crystals, which are not restricted by a Fermi level. Detail tight-binding calculations are presented in Supplementary Note 1.

We experimentally validate this mechanism in a two-dimensional photonic crystal by locally tailoring its boundary geometry, without globally deforming the lattice or invoking a higher-order bulk topological invariant. Near-field measurements directly reveal the corner-localized modes, which retain both their spectral isolation and spatial localization under positional and radius disorder. In contrast to conventional symmetry-dependent corner states protected by global lattice symmetries, the states reported here preserve their localization under local structural perturbations, whereas symmetry-protected corner states undergo rapid bandgap closure and lose corner localization under comparable disorder.

Results

Photonic design. To engineer flatband edge states within a topologically trivial bandgap, we start from a two-dimensional honeycomb lattice with a zigzag termination (Figs. 2a-2c). The structure comprises dielectric cylinders with lattice constant a, radius $r = 0.176a$, and relative permittivity ε=11.5. The dielectric profile is translationally invariant along the z direction, allowing the eigenmodes to be separated into transverse magnetic and transverse electric polarizations. In this work, we focus on transverse magnetic modes; transverse electric modes can be analyzed analogously. To visualize how the flatband edge state is displaced across the upper bulk bands and eventually relocated into a trivial bandgap, we calculate the surface density of states of semi-infinite photonic crystals with open boundaries (Figs. 2a-2c)[53]. When all cylinders have identical radii and the structure is unperturbed, the flatband edge state lies between two Dirac degeneracies at the K and K' points (Fig. 2a), in agreement with the tight-binding result (Fig. 1d). The slight bending of the flatband edge state originates from the intrinsic dispersion of the photonic crystal. In a Dirac semimetal system, a change in the boundary on-site mass can be readily implemented in photonic crystals by modifying the size of the boundary cylinders. Accordingly, we tailor only the outermost row of cylinders by reducing the boundary radius to $r_E = 0.8r$, as indicated by the white dashed line in Fig. 2b. As a result, the flatband edge state shifts upward into the bulk continuum. Upon further decreasing the boundary radius to $r_E = 0.50r$ (Fig. 2c), the flatband edge state traverses the upper bulk band and becomes fully isolated within the trivial bandgap. Additional surface density of states for different r_E are shown in Supplementary Note 2.

Programmable corner states. The isolation of the flatband edge state within a trivial bandgap, together with its strong frequency tunability enabled by local boundary tailoring, provides a direct and flexible route to realizing highly programmable corner states. This mechanism allows deterministic control over both the number of corner modes and their spectral positions within the bandgap, without altering the global lattice geometry or bulk topology. We independently introduce three corner modes in a triangular photonic crystal by locally tuning the radius ratio r_E/r of the cylinders located at the top, left, and right vertices (Fig. 2d). Specifically, the boundary radii of these three corner cylinders are set to $r_E = 0.5r$, $0.4r$, and $0.33r$, respectively. Figure 2e presents the eigenfrequency spectrum of the designed structure, where bulk and corner-localized modes are clearly distinguished. Each corner mode emerges at a distinct frequency within the bandgap, with normalized eigenfrequencies of 0.413, 0.446, and 0.475 corresponding to the left, top, and right corners, respectively. It should be noted that edge states associated with the finite lattice are not involved in the reported corner localization, since only the corner units are modified, while the bulk and edges remain unchanged. Figures 2f-2h display the electric field intensity distributions of these corner-localized modes under frequency-resolved excitation, confirming their strong spatial confinement. The simulation configuration is illustrated in Supplementary Note 3. These results demonstrate broadband spectral tunability of corner states achieved solely through local geometry modification. Crucially, this approach enables the formation of corner states without invoking global symmetry breaking or topological bandgap engineering. Instead, the corner states originate from a flatband edge state inherited from paired Dirac points and are selectively positioned inside a trivial bandgap through local boundary control. We also reveal that compressing the perfect electric conductor boundaries can also realize corner states in the trivial bandgap (see Supplementary Note 4).

Experimental identification. We fabricate photonic crystal samples to experimentally observe the corner states and benchmark the results against numerical simulations. The sample is a triangular photonic crystal with lattice constant a = 17 mm, consisting of 11 units along each side. The structure is composed of nonmagnetized yttrium iron garnet (YIG) cylinders with relative dielectric permittivity ε = 11.5, relative permeability μ = 1, and a radius r = 3 mm. To suppress radiation leakage into free space, the photonic crystal is sandwiched between two flat aluminum plates, which act as effective perfect electric conductor boundaries. The structure is excited by a broadband quasi-plane wave generated by a horn antenna, while the out-of-plane electric field E_z is detected using a probe antenna and recorded with a vector network analyzer (see Method and Supplementary Note 3). Figure 3a shows a top view of the fabricated photonic crystal without the top aluminum plate, where the three cylinders at the corners are modified to a reduced radius of r_1 = 1.4 mm. To suppress spurious resonances between the parallel metal plates, the surrounding region is filled with microwave-absorbing sponges.

The numerically calculated bulk band structure of the designed photonic crystal (Fig. 3b) exhibits a trivial bandgap between the second and third bands. Figure 3c presents the calculated eigenfrequencies of the finite triangular structure, clearly distinguishing bulk modes from corner-localized states residing inside the bandgap. To experimentally identify these corner states, the sample is illuminated by a plane wave incident from the + y direction, and transmission spectra are measured at two representative locations: the bulk center and the top corner of the structure. The corresponding spectrum of green (bulk) curve reveals a pronounced bandgap spanning from 6.89 to 8.83 GHz (Fig. 3d), evidenced by a sharp suppression of bulk transmission. This frequency range is consistent with the numerical predictions (Figs. 3b-3c).

Notably, a prominent transmission peak emerges at 7.48 GHz in the corner spectrum (orange curve in Fig. 3d), signaling the excitation of a localized corner mode. Near-field scanning at this frequency confirms strong field confinement at the top corner (Fig. 3f). For comparison, Figs. 3e and 3g display the measured electric field distributions corresponding to bulk modes in the lower and upper bands, respectively. Minor discrepancies between simulated and measured frequencies are attributed to fabrication tolerances in the YIG cylinder dimensions. We also note that the two bottom corners are not efficiently excited under plane wave illumination, owing to the absence of bulk or edge transport channels within the bandgap that could deliver energy to these corners. Overall, the experimental observations show good agreement with numerical simulations and unambiguously confirm the existence of programmable corners states.

Beyond this trivial-gap realization, we further demonstrate that the same local geometry engineering strategy can be extended to a topological Kagome lattice (see Supplementary Note 5), where tailored corner states are likewise constructed and observed through combined numerical design and experimental measurements. These results validate our central conclusion: in our scheme, corner-state formation is governed by local tailoring of flatband edge states, rather than by global symmetry breaking or higher-order bulk topological invariants.

Robust corner states. We further examine the robustness of the resulting states against structural perturbations, focusing on two representative types of disorder: position disorder and radius disorder[54–58]. Figures 4a-4c illustrate the unperturbed lattice together with the two disordered configurations. To quantify the disorder strength, we introduce a dimensionless fluctuation parameter δ. For position disorder (Fig. 4b), δ denotes the maximum displacement $\Delta\mathbf{x}$ of a cylinder center from its original position, defined by $|\Delta\mathbf{x}| = \delta a$. For radius disorder (Fig. 4c), δ characterizes the maximum deviation Δr from the nominal cylinder radius, defined as $|\Delta r| = \delta r$. In all simulations, the photonic crystal consists of dielectric cylinders with radius $r = 0.176a$ and relative permittivity $\varepsilon = 11.5$, while the corner cylinder is locally modified to a reduced radius of $r_E = 0.45r$.

Figures 4d and 4e present the calculated eigenfrequencies of bulk and corner modes as functions of the disorder strength δ for position and radius perturbations, respectively. In both cases, the bandgap and the corner-localized state remain clearly identifiable at low disorder levels. For position disorder (Fig. 4d), the bandgap persists even under relatively strong perturbations, with the corner state merging into the bulk continuum only when δ approaches 0.25. In contrast, for radius disorder (Fig. 4e), the bandgap closes at $\delta \approx 0.37$, and the corner state becomes indistinguishable from bulk modes when δ exceeds approximately 0.31. This comparison indicates that the bandgap is considerably more sensitive to radius fluctuations than to position displacements.

These results demonstrate that the corner states survive moderate levels of structural disorder, owing to the stability of the bandgap supported by intrinsic long-range structural order[55,59]. At sufficiently high disorder strengths, however, the long-range order of the photonic crystal is progressively destroyed, leading to the eventual loss of corner-state localization as the modes merge into the bulk spectrum. Notably, corner states protected by global symmetries are typically far more vulnerable to position disorder, since their formation relies on delicate interference conditions that are easily disrupted by random displacements. The disorder sensitivity of such symmetry-dependent corner states in topological Kagome lattice is illustrated in Supplementary Note 5. By contrast, the corner states realized here, derived from flatband edge states and not reliant on global symmetry protection, exhibit enhanced robustness against position perturbations.

Discussion and Conclusion

In summary, we have proposed and experimentally demonstrated a new class of robust corner states enabled by tailoring the flatband edge states originating from paired Dirac points. Rather than relying on global lattice-symmetry breaking, higher-order bulk topological invariants, or conventional topological bandgap engineering, our approach exploits local control of the boundary on-site mass in a honeycomb photonic crystal. This local tailoring deterministically shifts the flatband edge state across the upper bulk band and relocates it into a fully trivial bandgap, thereby inducing edge and corner localization. By modifying only the corner cylinders, we achieve spectra tunability and deterministic programmability of both the number and eigenfrequencies of corner states, without altering the global lattice geometry or

bulk properties. Disorder analysis further confirms that these corner states remain robust under moderate structural perturbations and exhibit enhanced tolerance to positional disorder.

Together, these results establish boundary-tailored flatband edge state as a new pathway for generating and programming corner states in Hermitian platforms. Owing to the scalability of photonic crystal platforms and the all-dielectric nature of our design, these robust corner states can be readily extended to the optical regime via standard nanofabrication techniques, providing a practical route toward on-chip, disorder-resilient photonic devices.

Methods

Numerical methods. The tight-binding model calculations in Figs. 1d-1g were performed in MATLAB using a two-dimensional honeycomb ribbon with $N = 11$ unit cells along the finite direction. The nearest-neighbor hopping amplitudes were set to t_1 and the boundary sites had an additional mass M_s. The surface density of states of the edge flatbands was obtained by calculating projected bandstructures and integrating eigenstates over the topmost and bottommost sites (see Supplementary Note 1). The corner states were calculated in a triangular geometry, where additional mass M_s was assigned to the topmost site. For the surface density of states associated with electromagnetic projected bandstructures, supercell structures were first constructed in COMSOL. The resulting eigenmatrices were then exported to MATLAB, where the transfer matrix method was utilized to calculate the surface density of states (see Supplementary Note 2 and Ref. 53). The optical modes and electromagnetic bandstructures were calculated by finite-element-method solver in COMSOL Multiphysics (see Supplementary Note 3 for the detailed boundary settings).

Microwave measurements. In our experimental setup, a vector network analyzer (Keysight P9374A) was used to excite and probe electromagnetic waves. For plane-wave incidence, the excitation port was connected to a horn antenna, while a monopole antenna was used for measurement. The spectra were measured from 5 GHz to 12 GHz with a resolution of 0.02 GHz.

For the transmission spectra measured at the bulk and corner positions in Fig. 3d, the sample was illuminated by a horn antenna from the $+y$ direction. A monopole probe antenna was inserted through the predrilled holes in the aluminum plate and positioned at the selected bulk and corner sites to detect the local electromagnetic field (see Supplementary Note 3). To obtain the electric-field distributions displayed in Figs. 3e–3g, we scanned the whole sample area in the x-y plane through the reserved holes one by one. The electromagnetic field at specific frequencies was then reconstructed.

Declarations

Acknowledgements

We acknowledge the financial support from the Science and Technology Project of Guangdong (2020B010190001), and the National Natural Science Foundation of China (12434016).

Author contributions

Z. J., J. C., and Z.-Y. L. conceived and designed this research project. Z. J. and J. C. performed the tight-binding calculations and electromagnetic simulations. Z. J. and Y. Z. fabricated the samples and conducted the experiments. Z. J., J. C., Z. D., and Z.-Y. L. analyzed the data and wrote the manuscript. J. C., Z. D., and Z.-Y. L. supervised the project.

Competing interests

The authors declare no competing interests.

References

1. Peterson CW, Benalcazar WA, Hughes TL, Bahl G (2018) A quantized microwave quadrupole insulator with topologically protected corner states. Nature 555:346–350
2. Noh J et al (2018) Topological protection of photonic mid-gap defect modes. Nat Photonics 12:408–415
3. Xie BY et al (2018) Second-order photonic topological insulator with corner states. Phys Rev B 98:205147
4. Banerjee R, Mandal S, Liew TCH (2020) Coupling between Exciton-Polariton Corner Modes through Edge States. Phys Rev Lett 124:63901
5. Ren Y, Qiao Z, Niu Q (2020) Engineering Corner States from Two-Dimensional Topological Insulators. Phys Rev Lett 124:166804
6. Chen R, Chen CZ, Gao JH, Zhou B, Xu DH (2020) Higher-Order Topological Insulators in Quasicrystals. Phys Rev Lett 124:036803
7. Wang B, Zhou X, Lin H, Bansil A (2021) Higher-order topological insulator phase in a modified Haldane model. Phys Rev B 104:L121108
8. Benalcazar WA, Cerjan A (2022) Chiral-Symmetric Higher-Order Topological Phases of Matter. Phys Rev Lett 128:127601
9. Ren B et al (2023) Theory of nonlinear corner states in photonic fractal lattices. Nanophotonics 12:3829–3838
10. Canyellas R et al (2024) Topological edge and corner states in bismuth fractal nanostructures. Nat Phys 20:1421–1428
11. Benalcazar WA, Bernevig BA, Hughes TL (2017) Quantized electric multipole insulators. Science 357:61–66
12. Langbehn J, Peng Y, Trifunovic L, von Oppen F, Brouwer PW (2017) Reflection-Symmetric Second-Order Topological Insulators and Superconductors. Phys Rev Lett 119:246401
13. Song Z, Fang Z, Fang C (2017) (*d*-2) -Dimensional Edge States of Rotation Symmetry Protected Topological States. *Phys. Rev. Lett.* 119, 246402

14. Schindler F et al (2018) Higher-order topological insulators. Sci Adv 4:eaat0346
15. Xu Y, Xue R, Wan S (2017) Topological Corner States on Kagome Lattice Based Chiral Higher-Order Topological Insulator. Preprint at https://arxiv.org/abs/1711.09202
16. Ezawa M (2018) Higher-Order Topological Insulators and Semimetals on the Breathing Kagome and Pyrochlore Lattices. Phys Rev Lett 120:026801
17. Mittal S et al (2019) Photonic quadrupole topological phases. Nat Photonics 13:692–696
18. Shi A et al (2021) Coupled cavity-waveguide based on topological corner state and edge state. Opt Lett 46:1089–1092
19. Gao YF et al (2022) Manipulation of coupling between topological edge state and corner state in photonic crystals. Opt Laser Technol 155:108387
20. Medina-Vázquez JA, González-Ramírez EY, Murillo-Ramírez JG (2023) Corner states in photonic higher-order Dirac semimetals. Phys Rev A 107:053511
21. Shi A et al (2024) Observation of Topological Corner State Arrays in Photonic Quasicrystals. Laser Photonics Rev 18:2300956
22. Ota Y et al (2019) Photonic crystal nanocavity based on a topological corner state. Optica 6:786–789
23. Chen X-D et al (2019) Direct Observation of Corner States in Second-Order Topological Photonic Crystal Slabs. Phys Rev Lett 122:233902
24. Xie B-Y et al (2019) Visualization of Higher-Order Topological Insulating Phases in Two-Dimensional Dielectric Photonic Crystals. Phys Rev Lett 122:233903
25. El Hassan A et al (2019) Corner states of light in photonic waveguides. Nat Photonics 13:697–700
26. Chen Y, Lu X, Chen H (2019) Effect of truncation on photonic corner states in a Kagome lattice. Opt Lett 44:4251–4254
27. Li M et al (2020) Higher-order topological states in photonic kagome crystals with long-range interactions. Nat Photonics 14:89–94
28. Shen S, Li C, Wu J-F (2021) Investigation of corner states in second-order photonic topological insulator. Opt Express 29:24045–24055
29. Kruk SS et al (2021) Nonlinear Imaging of Nanoscale Topological Corner States. Nano Lett 21:4592–4597
30. Serra-Garcia M et al (2018) Observation of a phononic quadrupole topological insulator. Nature 555:342–345
31. Xue H, Yang Y, Gao F, Chong Y, Zhang B (2019) Acoustic higher-order topological insulator on a kagome lattice. Nat Mater 18:108–112
32. Ni X, Weiner M, Alù A, Khanikaev AB (2019) Observation of higher-order topological acoustic states protected by generalized chiral symmetry. Nat Mater 18:113–120
33. Wu H et al (2023) Higher-Order Topological States in Thermal Diffusion. Adv Mater 35:2210825

34. Fukui T, Yoshida T, Hatsugai Y (2023) Higher-order topological heat conduction on a lattice for detection of corner states. Phys Rev E 108:024112
35. Liu Z et al (2024) Higher-Order Topological In-Bulk Corner State in Pure Diffusion Systems. Phys Rev Lett 132:176302
36. Imhof S et al (2018) Topolectrical-circuit realization of topological corner modes. Nat Phys 14:925–929
37. Liu S et al (2020) Octupole corner state in a three-dimensional topological circuit. Light Sci Appl 9:145
38. Olekhno NA et al (2022) Experimental realization of topological corner states in long-range-coupled electrical circuits. Phys Rev B 105:L081107
39. Pelegrí G, Marques AM, Ahufinger V, Mompart J, Dias RG (2019) Second-order topological corner states with ultracold atoms carrying orbital angular momentum in optical lattices. Phys Rev B 100:205109
40. Zhang W et al (2020) Low-threshold topological nanolasers based on the second-order corner state. Light Sci Appl 9:109
41. Kim H-R et al (2020) Multipolar lasing modes from topological corner states. Nat Commun 11:5758
42. Xie X et al (2020) Cavity Quantum Electrodynamics with Second-Order Topological Corner State. Laser Photon Rev 14:1900425
43. Zhong H et al (2021) Theory of topological corner state laser in Kagome waveguide arrays. APL Photonics 6:040802
44. Wu J et al (2023) Higher-order topological polariton corner state lasing. Sci Adv 9:eadg4322
45. Rao M et al (2024) Single photon emitter deterministically coupled to a topological corner state. Light Sci Appl 13:19
46. Liang L et al (2022) Rainbow trapping based on higher-order topological corner modes. Opt Lett 47:1454–1457
47. AbdelAll N, Almokhtar M, Khouqeer G, Abood I, El. Soliman S (2024) Rainbow Trapping with Engineered Topological Corner States and Cavities in Photonic Crystals. Adv Quantum Technol 7:2400050
48. Rivero JDH, Fleming C, Qi B, Feng L, Ge L (2023) Robust Zero Modes in Non-Hermitian Systems without Global Symmetries. Phys Rev Lett 131:223801
49. McCall S, Platzman P, Dalichaouch R, Smith D, Schultz S (1991) Microwave propagation in two-dimensional dielectric lattices. Phys Rev Lett 67:2017–2020
50. Fedele F, Yang J, Chen Z (2005) Defect modes in one-dimensional photonic lattices. Opt Lett 30:1506–1508
51. Makasyuk I, Chen Z, Yang J (2006) Band-Gap Guidance in Optically Induced Photonic Lattices with a Negative Defect. Phys Rev Lett 96:223903

52. Reisner M, Bellec M, Kuhl U, Mortessagne F (2021) Microwave resonator lattices for topological photonics [Invited]. Opt Mater Express 11:629–653
53. Sha Y, Xia M, Lu L, Yang Y (2025) Efficient algorithms for the surface density of states in topological photonic and acoustic systems. Nat Comput Sci 5:1192–1201
54. Li Z-Y, Zhang X, Zhang Z-Q (2000) Disordered photonic crystals understood by a perturbation formalism. Phys Rev B 61:15738
55. Li Z-Y, Zhang Z-Q (2000) Fragility of photonic band gaps in inverse-opal photonic crystals. Phys Rev B 62:1516–1519
56. Frei WR, Johnson HT (2004) Finite-element analysis of disorder effects in photonic crystals. Phys Rev B 70:165116
57. Kwan K-C, Zhang X, Zhang Z-Q, Chan CT (2003) Effects due to disorder on photonic crystal-based waveguides. Appl Phys Lett 82:4414–4416
58. Chen J, Qin Q, Peng C, Li Z-Y (2022) Robust topological one-way edge states in radius-fluctuated photonic Chern topological insulators. Opt Express 30:21621–21633
59. Liew SF, Cao H (2010) Optical properties of 1D photonic crystals with correlated and uncorrelated disorder. J Opt 12:024011

Figures

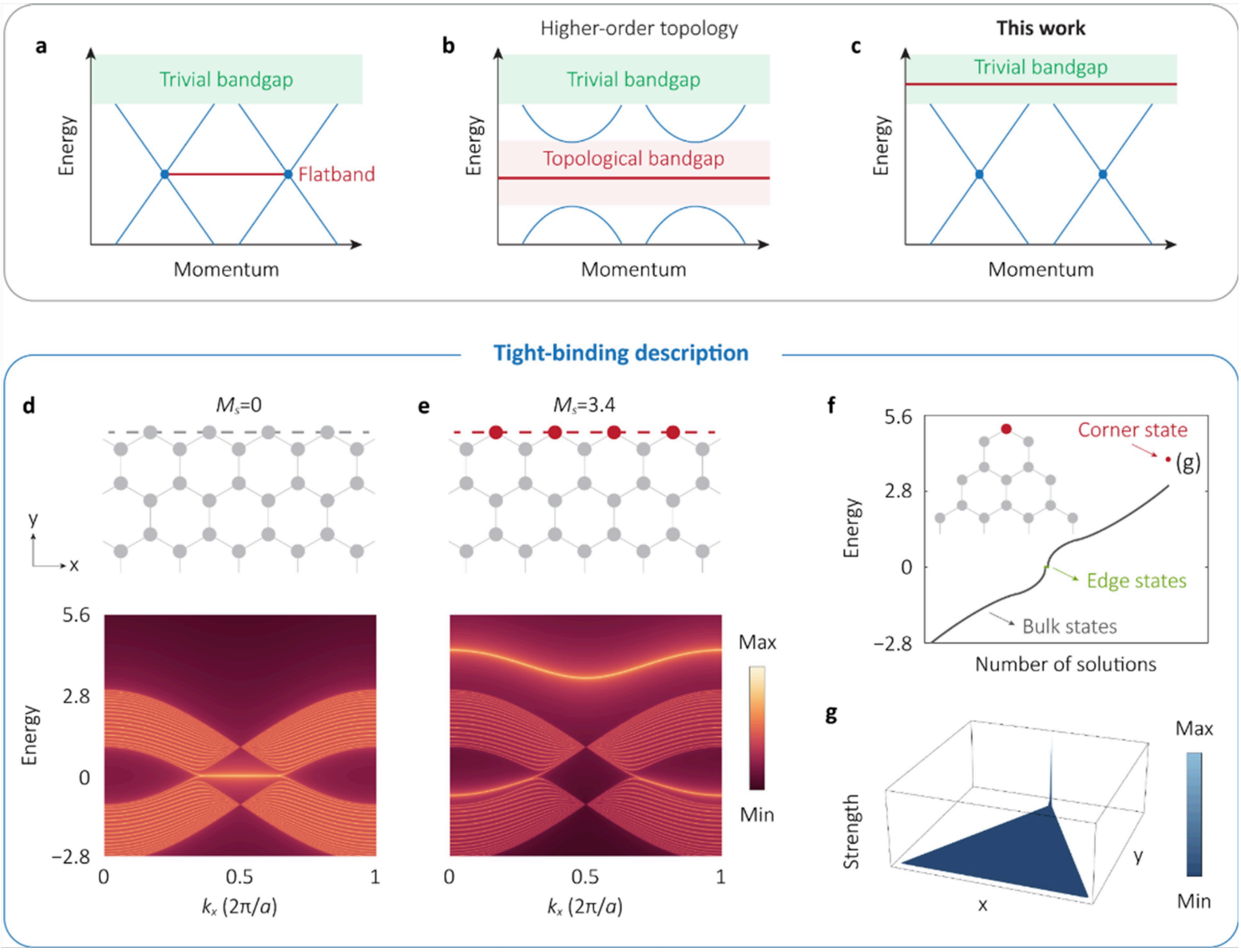


Figure 1

Robust corner states derived from Dirac-connected flatband edge states. (a-c) Two routes to creating edge and corner states from the flatband edge states of a Dirac semimetal. (a) Projected band structure of a Dirac semimetal, showing flatband edge states connecting the boundary projections of a pair of bulk Dirac points. (b) Lifting the Dirac-point degeneracy opens a topologically nontrivial bandgap, within which the Dirac-connected edge states persist and give rise to topological boundary states. (c) Without lifting the Dirac-point degeneracy, relocating the flatband edge states into a separate, topologically trivial bandgap also produces spectrally isolated edge and corner states. (d-g) Tight-binding description of the proposed mechanism. (d) Lattice geometry and projected band structure of the Dirac semimetal; the color scale denotes the surface density of states. (e) Boundary engineering shifts the Dirac-connected flatband edge states through the upper bulk band and into a trivial bandgap. (f) Finite rhombic lattice and its eigenvalue spectrum. (g) Spatial field distribution of the corner-state eigenmode.

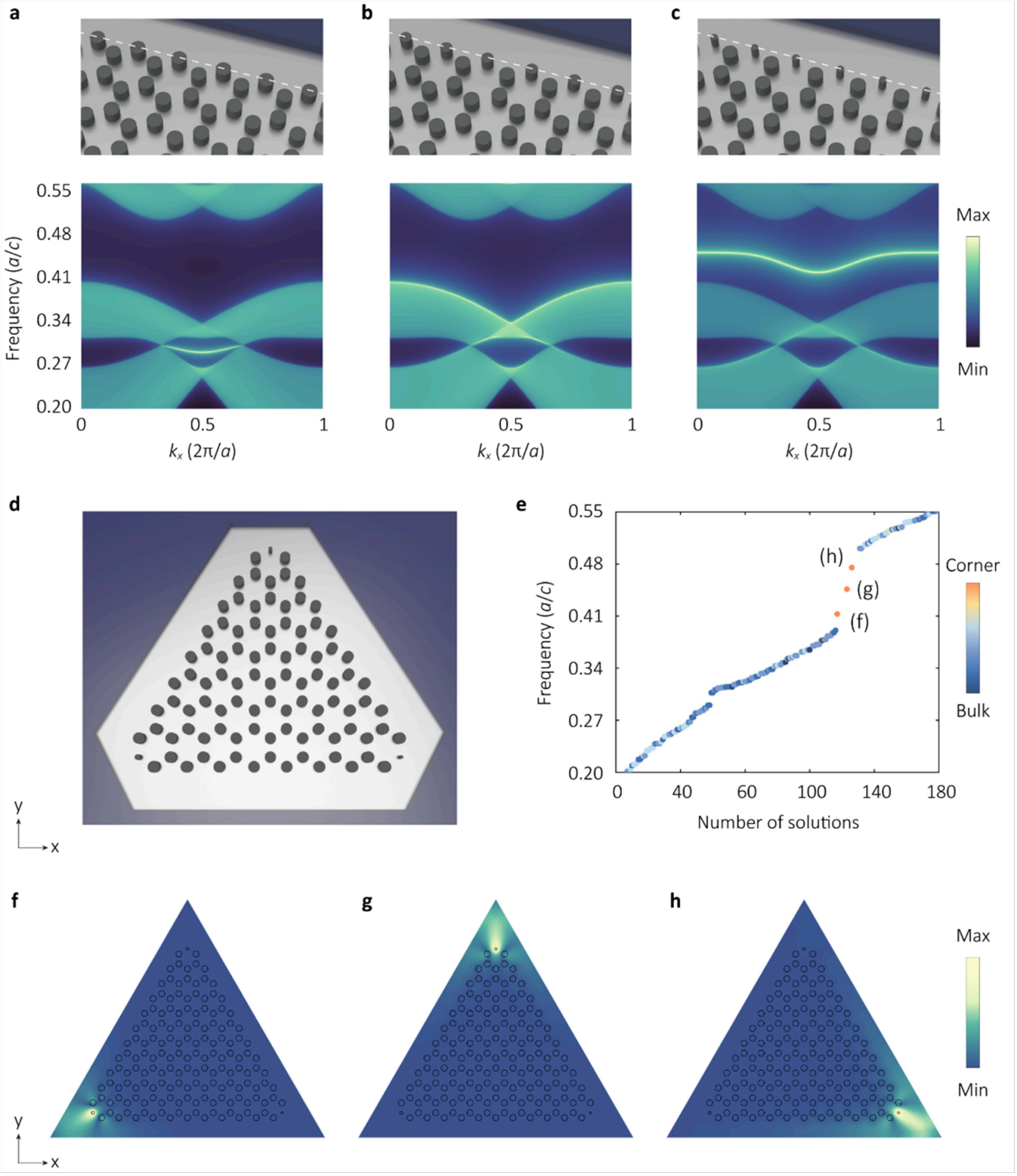


Figure 2

Programmable corner states in photonic crystals. (a-c) Close-up views of the sample geometry and the corresponding projected bandstructures; the color scale denotes the surface density of states. The radius of the bulk is $r = 0.176a$, while the radius of the boundary cylinders (white dashed lines) is $r_E = r$ in (a), $r_E = 0.8r$ in (b), and $r_E = 0.5r$ in (c), respectively. (d) Schematic of a triangular photonic crystal placed on an aluminum plate. The surrounding blue regions denote absorbing materials used to suppress

unwanted reflections. (e) Eigenfrequency spectrum of the triangular photonic crystal, where bulk and corner states are distinguished. (f-h) Eigenmodal field distributions of the corner states, which appear at different frequencies due to the unequal cylinder radii at the three corners.

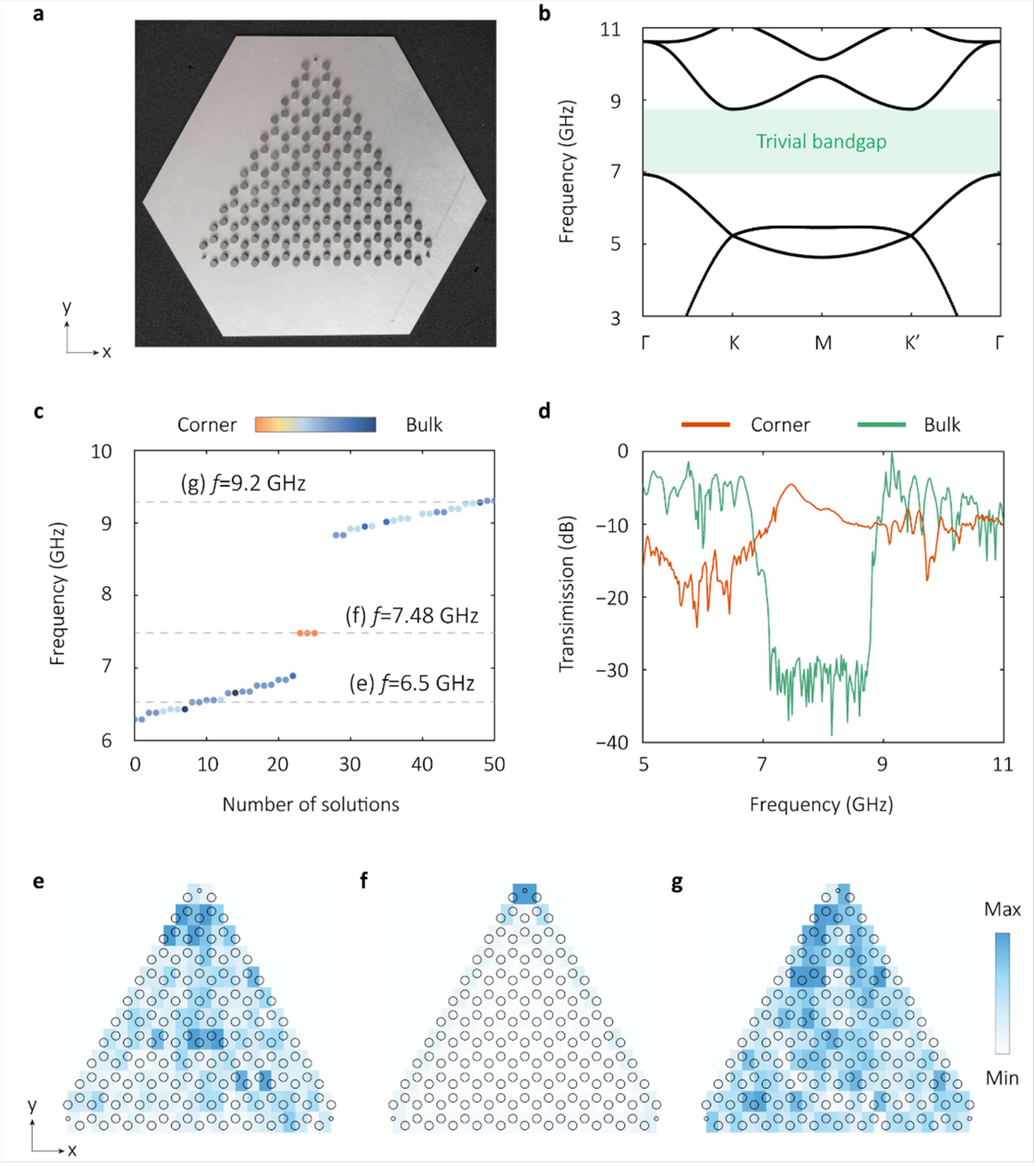


Figure 3

Observation of topological corner states. (a) Top view of the fabricated triangular photonic crystal without the top aluminum plate. (b) Numerically calculated bulk band showing a trivial bandgap (shaded region). (c) Calculated eigenfrequencies of bulk and corner states for the finite triangular structure. (d) Measured transmission spectra at bulk (green) and corner (orange) positions under plane-wave excitation. (e-g) Measured electric-field distributions at representative frequencies: (e) f = 6.5 GHz (bulk state), (f) f = 7.48 GHz (corner state), and (g) f = 9.2 GHz (bulk state).

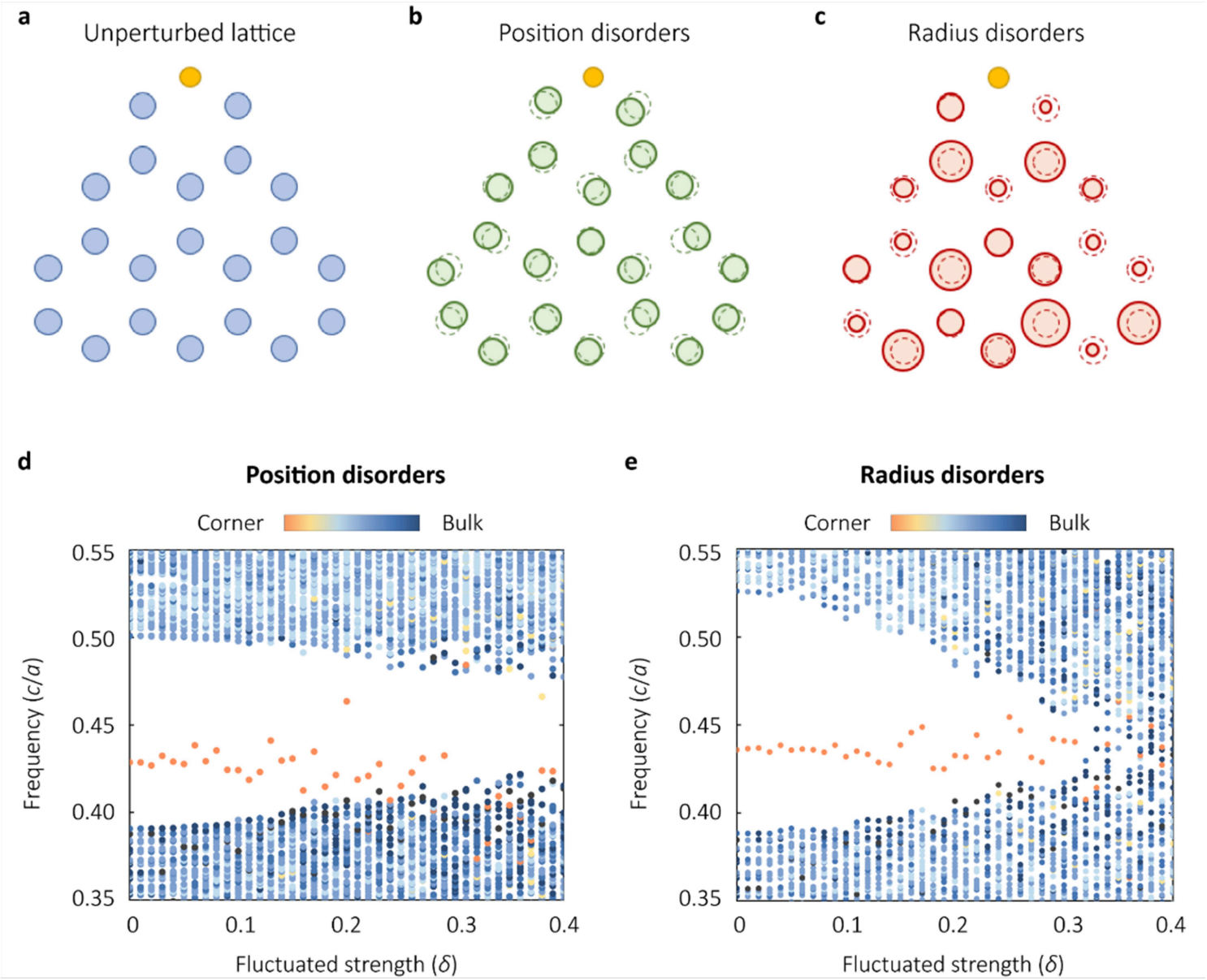


Figure 4

Robustness of corner states under structural disorder.(a)-(c) Schematic diagrams of photonic crystal configurations: (a) Without perturbation. (b) Position disorders. (c) Radius disorders. (d)-(e) Eigenfrequencies of corner and bulk modes as a function of disorder strength for (d) position disorders and (e) radius disorders.

Supplementary Files

This is a list of supplementary files associated with this preprint. Click to download.

- SupplementaryInformation.docx